NANO LETTERS
Letter
Cite This: Nano Lett. 2019, 19, 2020−2026
pubs.acs.org/NanoLett

Stepwise Ligand-induced Self-assembly for Facile Fabrication of Nanodiamond−Gold Nanoparticle Dimers via Noncovalent Biotin−Streptavidin Interactions

Miu Shan Chan,[†] Renate Landig,[‡,§] Joonhee Choi,[‡,∥] Hengyun Zhou,[‡] Xing Liao,[§] Mikhail D. Lukin,[‡] Hongkun Park,[‡,§] and Pik Kwan Lo*[,†,⊥]

[†]Department of Chemistry, City University of Hong Kong, Tat Chee Avenue, Kowloon Tong, Hong Kong SAR, China
[‡]Department of Physics, [§]Department of Chemistry and Chemical Biology, and [∥]School of Engineering and Applied Sciences, Harvard University, Cambridge, Massachusetts 02138, United States
[⊥]Key Laboratory of Biochip Technology, Biotech and Health Care, Shenzhen Research Institute of City University of Hong Kong, Shenzhen 518057, China

Supporting Information

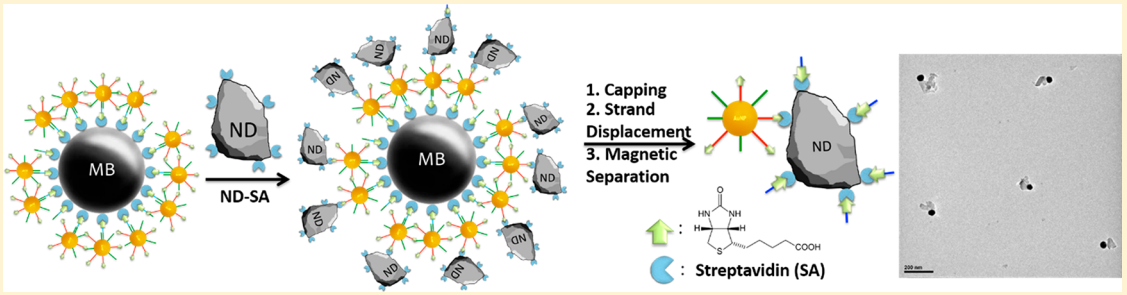

ABSTRACT: Nanodiamond−gold nanoparticle (ND-AuNP) dimers constitute a potent tool for controlled thermal heating of biological systems on the nanoscale, by combining a local light-induced heat source with a sensitive local thermometer. Unfortunately, previous solution-based strategies to build ND-AuNP conjugates resulted in large nanoclusters or a broad population of multimers with limited separation efficiency. Here, we describe a new strategy to synthesize discrete ND-AuNP dimers via the synthesis of biotin-labeled DNA-AuNPs through thiol chemistry and its immobilization onto the magnetic bead (MB) surface, followed by reacting with streptavidin-labeled NDs. The dimers can be easily released from MB via a strand displacement reaction and separated magnetically. Our method is facile, convenient, and scalable, ensuring high-throughput formation of very stable dimer structures. This ligand-induced self-assembly approach enables the preparation of a wide variety of dimers of designated sizes and compositions, thus opening up the possibility that they can be deployed in many biological actuation and sensing applications.

KEYWORDS: *biotin−streptavidin interactions, nanodiamond, gold nanoparticle, particle dimers, dual-functional*

Integration of different building blocks with desired electronic, optical, magnetic, and collective properties into a single material platform with multiple functions is of great importance in various emerging applications.[1−5] Owing to its functionalization versatility, chemical inertness, relatively low cytotoxicity, and high affinity to biomolecules,[6] nanodiamonds (ND) have emerged as a promising vehicle for drug/gene delivery.[7,8] Particularly, the negatively charged nitrogen-vacancy (NV^-) centers in NDs are exceptionally photostable with broad emission wavelength and reasonable lifetime, which is attractive for long-term particle tracking and bioimaging.[9] The electronic spin state in NV^- center can be optically prepared as well as detected, thus providing a material basis for highly sensitive nanoscale magnetometry.[10,11] These combined properties make NDs superior to other materials as quantum sensors at the interface of biology and physics.[12,13] Recently, several temperature sensing techniques based on NV^- centers have been demonstrated.[14−16] By attaching this temperature sensor to other nanomaterials that provide localized heating, malignant cells can potentially be selectively killed without damaging surrounding tissue.[17] Besides, specific gene expression could be accurately controlled by simultaneously measuring and controlling the subcellular thermal gradient.[18] Gold nanoparticles (AuNPs) can serve as local heaters at the nanoscale due to their visible plasmonic resonance that can be tuned via the shape and size of the nanoparticle.[19] Hybridizing a single AuNP with a single ND realizes a dual-functional nanodevice that achieves highly localized heating and

Received: January 10, 2019
Revised: February 13, 2019
Published: February 19, 2019

DOI: 10.1021/acs.nanolett.9b00113
Nano Lett. 2019, 19, 2020−2026

Scheme 1. Synthesis of (a) Biotin-labeled, DNA-functionalized Gold Nanoparticle AuNP-$D_{1b'2}$ and (b) DNA-functionalized Magnetic Bead MB-D_{1ab}, and (c) Formation of ND-AuNP Hybrids after Detaching from the MB via Strand Displacement Approach

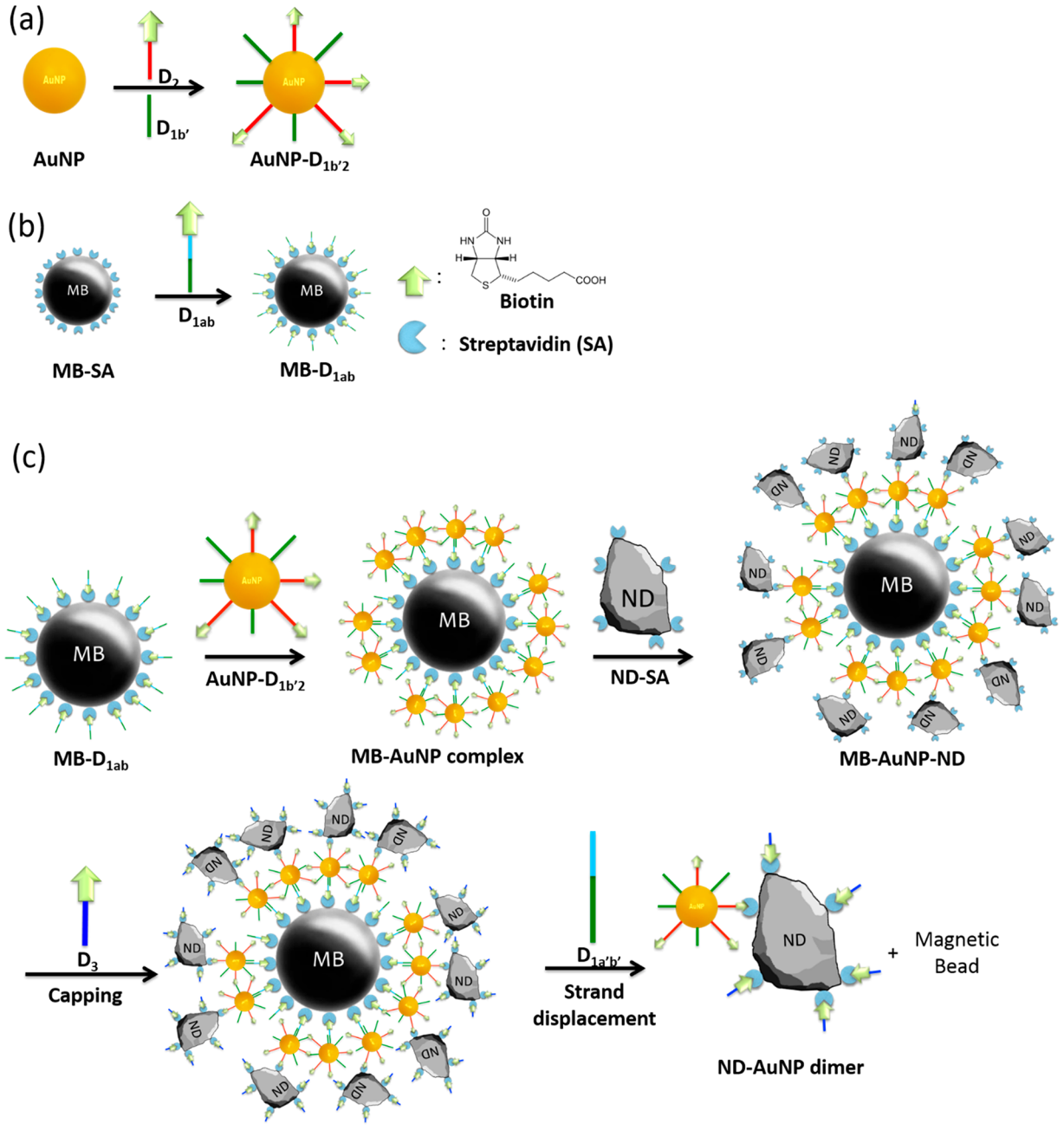

simultaneous in situ detection of temperature at the nanoscale, beneficial for real-time control and monitoring of local temperatures within a biological specimen as well as controlled plasmon-based photothermal therapy with high therapeutic accuracy.[20]

Several strategies have been applied to generate ND-AuNP hybrids.[21] For example, a noncovalent approach was used to couple different sizes of AuNPs with NDs via DNA hybridization.[22] Recently, Liu et al. generated ND-AuNP conjugates in a wide range of size distributions using an amine-carboxylic acid cross-linking strategy catalyzed by 1-ethyl-3-(3-(dimethylamino)propyl) carbodiimide hydrochloride-*N*-hydroxysuccinimide:[23] in this approach, carboxylated-NDs and AuNPs were covalently linked with amine-functionalized human serum albumin (HAS) via amide bonds, and analytical ultracentrifugation was used to isolate the ND-AuNP conjugates within certain size ranges. Covalent attachment of amine-functionalized AuNPs with carboxylated-NDs via carbodiimide chemistry was also employed to generate the contrast agents.[24] Tsai et al. fabricated diamond−gold nanohybrids by coating a few gold nanorods onto the poly-L-arginine-functionalized NDs via physical adsorption and demonstrated reliable temperature measurements using them.[21] Unfortunately, to date, all these synthetic approaches for diamond−AuNP conjugates resulted in large nanoclusters or a mixture of dimers, trimers, and/or multimers. To ensure controlled heating, a new strategy for high yield fabrication of discrete ND-AuNP dimers is highly desirable.

DOI: 10.1021/acs.nanolett.9b00113
Nano Lett. 2019, 19, 2020−2026

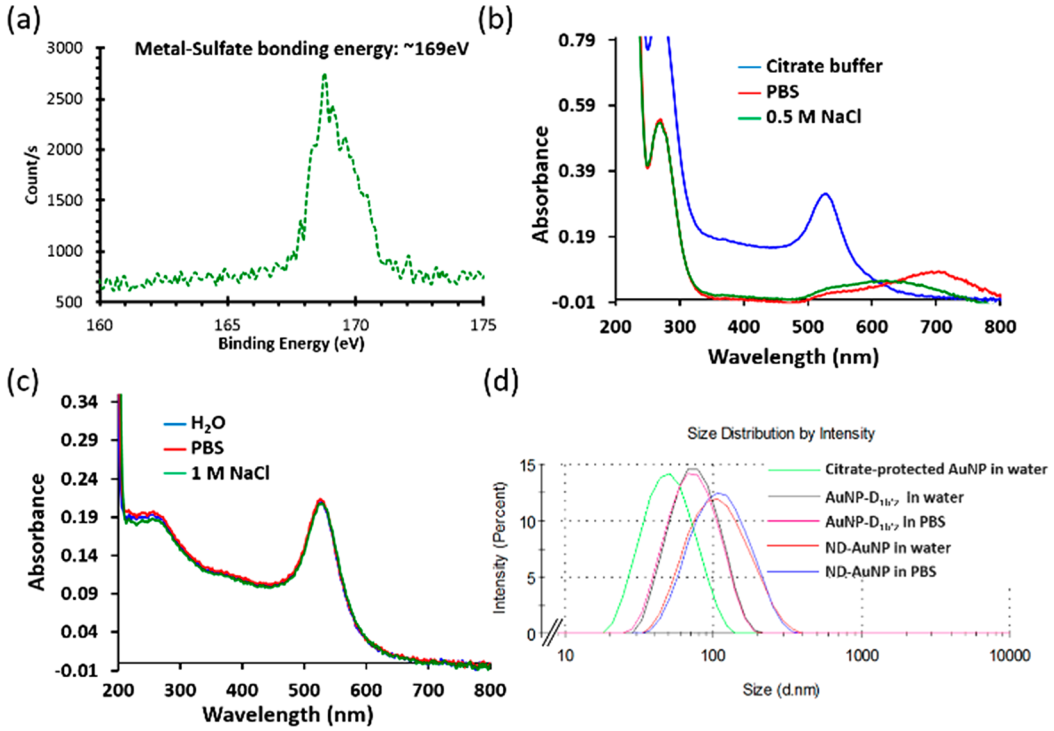

Figure 1. (a) XPS analysis of the bonding between thiol-functionalized oligonucleotide and AuNP, UV−vis analysis of (b) citrate-protected AuNPs incubated for 30 min and (c) AuNP-$D_{1b'2}$ incubated for 48 h in different solution conditions, and (d) DLS analysis of the size distribution by intensity of different samples in water or in buffer.

Herein, we construct a designed ND-AuNP dimer through a stepwise ligand-induced self-assembly approach (Scheme 1). First, biotin-labeled DNA-encoded AuNPs are immobilized onto DNA-labeled MB by means of single-target DNA hybridization. Second, streptavidin-labeled NDs are added to form individual MB-AuNP-ND complexes via noncovalent bonds. A strand displacement reaction is used to release discrete ND-AuNP dimers from MB in buffer solutions. As compared to other fabrication approaches, this strategy is scalable and assures high-yield synthesis of dimer structures (~50%) because no time-consuming purification step is required. The same synthetic strategy can be used to prepare a variety of dimers with designated sizes and compositions.

Generally, the commercially available citrate-coated AuNPs are very unstable and tend to aggregate in buffer systems. To address this problem, we functionalized AuNPs with negatively charged oligonucleotides, thus generating NPs with excellent stability at high ionic strength.[25] The self-recognition property and versatile functionalization of DNA at both ends enable a diverse linkage between two targets. In our experiments, two different sequences of 5′ thiol-labeled DNA strands, $D_{1b'}$ and D_2, were added in a mole ratio of 1:1 to the solution of 30 nm diameter AuNPs (Scheme 1a). The linking strand, $D_{1b'}$, and the target-capture strand, D_2, randomly attach onto AuNP surface through metal−sulfur bonds to form AuNP-$D_{1b'2}$. The biotin functional group at the 3′-end of D_2 serves as an attachment point for grafting streptavidin-labeled NDs. Centrifugation was used to remove the unreacted DNA strands. The X-ray photoelectron spectroscopy (XPS) spectrum showed a characteristic peak at −169 eV for metal−sulfate bonds (Figure 1a). As compared to citrate-coated AuNPs in PBS and in 1 M NaCl solutions, neither red shifts nor a decrease of the plasmonic absorption peak of AuNP-$D_{1b'2}$ at ~532 nm was observed (Figure 1b,c). These results indicated that DNA-protected AuNPs exhibit excellent colloidal stability in buffer solutions even after 48 h. The particle size of AuNP-$D_{1b'2}$ was characterized by dynamic light scattering (DLS) analysis (Figure 1d). After coating the citrate-coated AuNPs with DNA strands, its average diameter changed from 53.01 to 77.69 nm with polydispersity index of ~0.13. This enhancement is consistent with the size of added $D_{1b'}$ and D_2 strands, which are with 66 nucleobases in length. No significant size deviation was observed when AuNP-$D_{1b'2}$ was dispersed in either water or PBS, further confirming the absence of aggregation.

To facilitate a simple purification procedure after conjugation, MBs were used as solid supports. To cross-link AuNP-$D_{1b'2}$ and MB, biotin-labeled DNA strands D_{1ab} were added to the streptavidin-functionalized MBs (MBs-SA) in Tris-NaCl buffer to form MB-D_{1ab} via biotin−streptavidin interaction (Scheme 1b). The sequences of D_{1ab} strand are designed to be partially complementary to the linking strand $D_{1b'}$. Pure MB-D_{1ab} was obtained via magnetic separation. The successful formation of MB-D_{1ab} was confirmed by fluorescence measurements after adding Cy3-labeled $D_{1a'b'}$ that is fully complementary to D_{1ab} (Figure S1 in the Supporting Information). When AuNP-$D_{1b'2}$ was reacted with MB-D_{1ab} in PBS-TAMg buffer at room temperature for 6 h with gentle vortexing, $D_{1b'}$ on AuNP-$D_{1b'2}$ is partially hybridized to the terminal of D_{1ab} on MB-D_{1ab} to form MB-AuNP complexes (Scheme 1c). Pure MB-AuNP complexes were obtained after several rounds of washing and magnetic separation. The unbound biotin-functionalized D_2 on AuNP was preserved for further coupling. The transmission electron microscope (TEM) images show large amounts of 30 nm AuNPs coated on MB's surface (Figure 2a). We found that 0.42 pmol of AuNP-$D_{1b'2}$ was successfully captured by 1 mg of MB-D_{1ab} by determining the concentration of AuNP-$D_{1b'2}$ supernatant

DOI: 10.1021/acs.nanolett.9b00113
Nano Lett. 2019, 19, 2020−2026

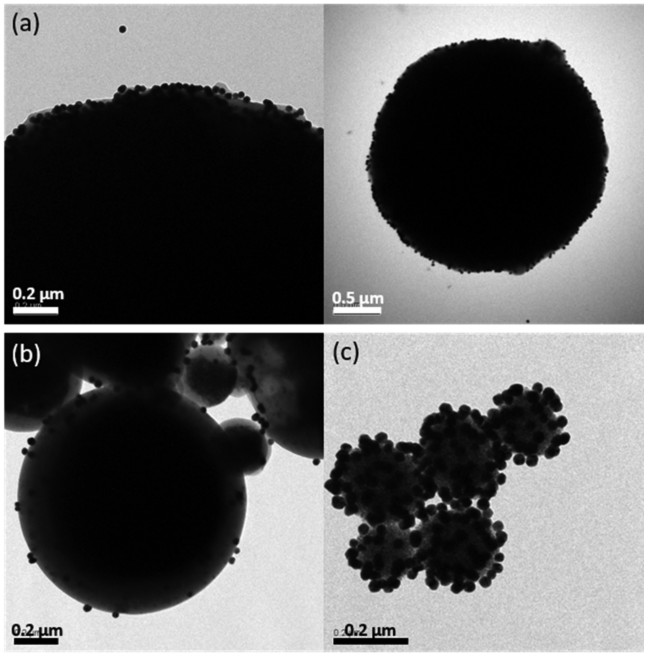

Figure 2. TEM images of MB-AuNP complex by coating 30 nm AuNPs on (a) 3 μm, (b) 0.8 μm, and (c) 0.3 μm MB.

before and after the reaction via UV−vis studies (Figure S2 in the Supporting Information). We also explored different sizes of MB (e.g., 0.3, 0.8, and 3 μm). It is important to note that increasing the size ratio of the magnetic bead to gold nanoparticle could prevent the self-aggregation of MB-AuNP complexes for the following reason: the size distribution of 3 μm MB is more even than the other two sizes of MBs, resulting in highly monodispersed and spherical particles with the diameter of 3 μm (Figure 2a). The 0.3 and 0.8 μm MBs, which are in a wide range of size distribution, would prefer to aggregate by themselves to become larger clusters in solution phases (Figures 2 and S3, Supporting Information).

Once the MB-AuNP was on hand, excess streptavidin-functionalized NDs (NDs-SA) were added. The free biotin groups on AuNP-$D_{1b'2}$ further react with 40 nm ND-SA via biotin−streptavidin interaction to generate MB-AuNP-ND (Scheme 1c). Excess unreacted ND-SAs were removed by magnetic separation. To prevent the unbound SAs on NDs from further reacting with biotin-labeled AuNPs after releasing from MBs, a short biotinylated-single-stranded DNA, D3, was added subsequently to cap all the unreacted SA sites in the complexes. Nonspecific binding of NDs to the MB surface did not occur, as was confirmed by adding 40 nm ND-SA to the MB-D_{1ab} and observing no ND coating (Figure S4 in the Supporting Information). Finally, large amount of eraser DNA, $D_{1a'b'}$, which is fully complementary to D_{1ab}, was added in PBS-TAMg buffer to release ND-AuNP dimers from MB via a strand displacement reaction.

Polyacrylamide gel electrophoresis (PAGE) analysis was used to confirm DNA hybridization between D_{1ab} and $D_{1b'}$ (Figure S5, lanes 1 to 3) and to verify the strand displacement approach to release the bound $D_{1b'}$ by the addition of eraser DNA strand $D_{1a'b'}$ (Figure S5 in the Supporting Information, lanes 4 to 6). Their hybridization is highly efficient at room temperature even without annealing for the following two reasons: In our design, D_{1ab} hybridizes with $D_{1b'}$ via 15 base pairing interaction, while D_{1ab} hybridizes with $D_{1a''}$ via 23 base pairing interaction. The designed sequence of either D_{1ab}, $D_{1b'}$, or $D_{1a'b'}$ for self-complementarity is not favorable. Second, we found that the melting temperature (T_m) of a pair of D_{1ab} and $D_{1b'}$ is ~ 60 °C, while the T_m of a pair of D_{1ab} and $D_{1a'b'}$ is ~66 °C (Figure S6 in the Supporting Information). These T_m values are much higher than room temperature. Therefore, no annealing process is required for efficient hybridization.

Due to the steric effect of AuNPs on MBs, streptavidin-labeled NDs are restricted to interact with only one of the biotin sites of AuNP to form dimeric nanostructures with a relatively high yield. In contrast, as shown in Figure S7 in the Supporting Information, large nanoclusters are formed by directly mixing ND-SA with AuNP-$D_{1b'2}$ without using the MB solid support, and only 30 nm AuNPs are released from MB under the same synthetic strategy if AuNPs are fully coated with $D_{1b'}$ only (without the biotin coating). Careful analysis of TEM images revealed that ND-AuNP dimers are stable in

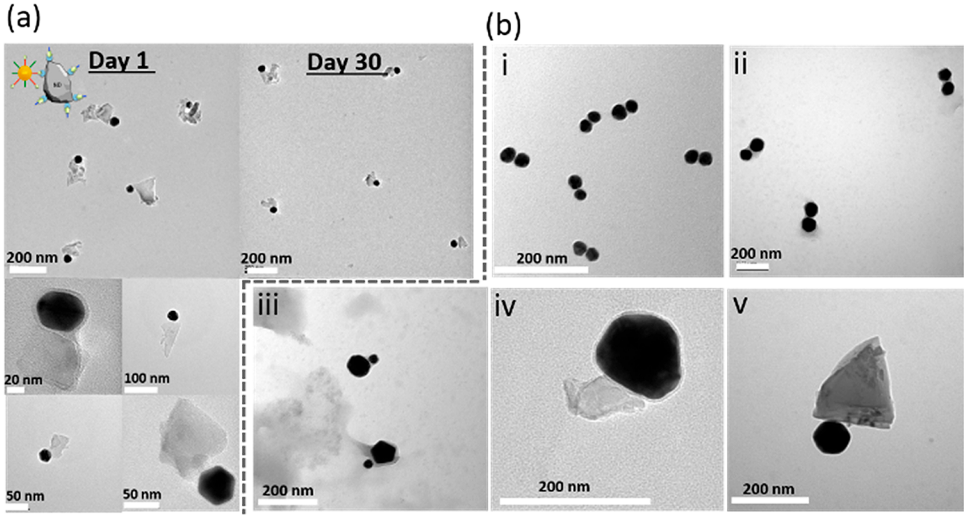

Figure 3. TEM images of (a) 40 nm ND−30 nm AuNP dimers after a month of storage, and (b) different combinations of dimers: (i) 30 nm AuNP−30 nm AuNP, (ii) 80 nm AuNP−80 nm AuNP, (iii) 30 nm AuNP−80 nm AuNP, (iv) 40 nm ND−80 nm AuNP, and (v) 200 nm ND−80 nm AuNP.

DOI: 10.1021/acs.nanolett.9b00113
Nano Lett. 2019, 19, 2020−2026

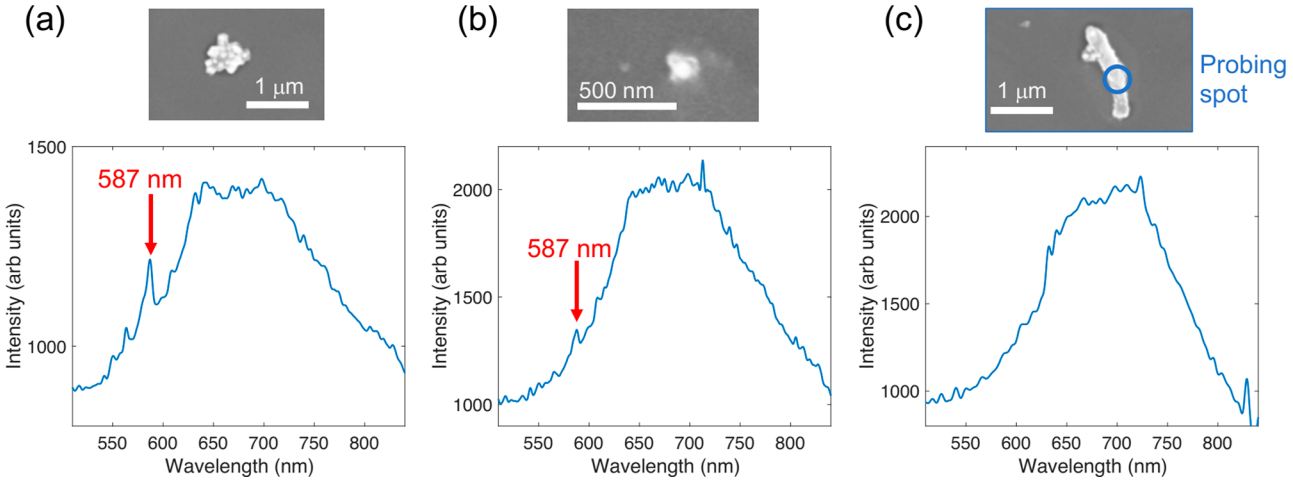

Figure 4. Fluorescence spectra under green excitation and SEM images of (a) a 40 nm ND with 80 nm AuNP cluster, (b) a 40 nm ND−80 nm AuNP dimer, and (c) ND clusters without AuNPs.

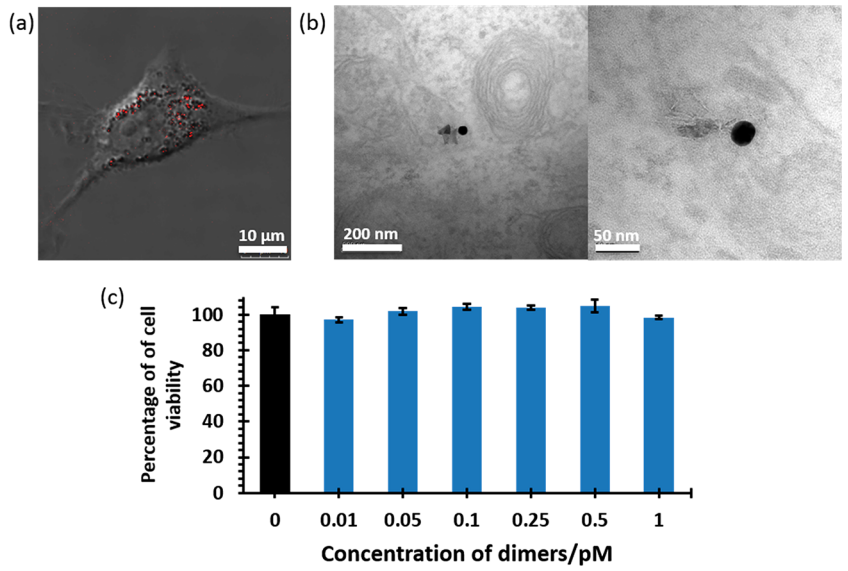

Figure 5. (a) Confocal fluorescence imaging of HeLa cells loaded with 40 nm ND−30 nm AuNP dimers after 24 h incubation. λ_{ex} = 633 nm and λ_{em} = 650−800 nm. Scale bar is 10 μm. (b) TEM images of dimer-treated HeLa cell showing dimers distributed inside HeLa cells. (c) Cytotoxicity of ND-AuNP dimers in the HeLa cells as a function of concentrations.

solution even after a month of storage and their size remains unchanged, staying in a range of 100−200 nm (Figures 3a and S8, Supporting Information). DLS analysis after a month of storage further confirmed ND-AuNP dimers are still well-dispersed with an average diameter of 118.6 nm in water and 120.8 nm in PBS buffer with polydispersity index of ∼0.163 (Figure 1d). These results strongly indicate that dimers are highly stable in PBS buffer for storage at 4 °C without aggregation. Comparing to DNA-assembly approach, particle conjugation must be performed in the presence of ion such as Mg^{2+}. Without the Mg^{2+} ions, DNA linkers between ND and AuNP will disassemble easily under sonication for a few minutes even in ice bath. In this new approach, it is well-known that streptavidin binds to biotin with very high affinity. Thus, the streptavidin−biotin binding interaction between ND and AuNP is much more stable in aqueous solution even without any cations and/or under short period of sonication in ice bath. Overall, highly stable particle dimers can be simply synthesized with a relatively high yield (∼50%, Figure S9 in the Supporting Information) and do not degrade after 30 min of mechanical sonication.[26,27]

Additionally, different combinations of particle dimers including 30 nm AuNP−30 nm AuNP, 80 nm AuNP−80 nm AuNP, 30 nm AuNP−80 nm AuNP, 40 nm ND−80 nm AuNP, and 200 nm ND−80 nm AuNP have also been successfully prepared, verifying the broad applicability of this synthetic strategy (Figures 3b and S10, Supporting Information). In general, comparing to heterodimers, the synthetic yield of homodimers (AuNP−AuNP) is much higher. It is because the surface of gold nanoparticle (AuNP-SA) was loaded with a large amount of streptavidin-labeled DNAs, e.g., >100 streptavidin molecules. The attachment point between biotin-labeled AuNPs (AuNP-$D_{1b'2}$) and AuNP-SA is much more than that of the commercially available ND-SA, which only has ∼8−10 streptavidin molecules on its surface. Additionally, nanodiamond with irregular shape results in poor control in the spacing during conjugation and reduces the

DOI: 10.1021/acs.nanolett.9b00113
Nano Lett. 2019, 19, 2020−2026

conjugation efficiency, such as blocking the neighbor nanoparticles conjugating with another approaching AuNP.

In order to distinguish the fabricated high-yield ND-AuNP dimers from the mostly bare NV centers and gold nanoparticles in the solution, their fluorescence spectrum was analyzed. Under green excitation at 532 nm, ND-AuNP clusters and ND-AuNP dimer exhibited a characteristic emission peak at 587 nm in addition to the typical broad emission spectrum from 550 to 800 nm stemming from NV centers (Figure 4), confirming that it is feasible to identify ND-AuNP complexes optically. We strongly believe that the 587 nm peak is associated with plasmon-enhanced surface fluorescence of the AuNP under the green excitation at 532 nm but does not originate from a Raman shift from the ND for the following two reasons: First, we also observe such a characteristic peak from an isolated AuNP, namely, even in the absence of a ND,[28] suggesting that it is not related to the ND. Second, the formation of a graphite layer is largely suppressed during the annealing process of the ND, typically performed at 700−800 °C to increase the number of NVs. It is known that diamond-to-graphite (sp^3-to-sp^2) conversion can be avoided when the annealing temperature is held below 1000 °C.[29] In fact, AuNPs can affect NV emission, either enhancing or reducing the NV emission rate via plasmonic enhancement or ohmic absorption, respectively. The relative strength between these two effects can be systematically controlled by the size of the AuNP, which is commonly quantified by comparing scattering and absorption cross sections of the AuNP for a given diameter. According to known literature, the 80 nm AuNPs used in our experiments are expected to show similar magnitudes of the cross sections, implying equal contributions from the two competing effects.[30] This is consistent with our experimental observation in which we could not identify any obvious correlation of the NV photon count with the presence/absence of AuNPs.

The application of ND-AuNP dimer as a robust thermometer−heater platform for studying cellular functions requires biocompatibility and efficient cellular uptake. In order to test the utility of ND-AuNP dimer in this context, we incubated HeLa cells with 19 fM of 40 nm ND-30 nm AuNP dimers for 24 h and studied them using confocal fluorescence imaging and TEM studies (Figures 5a,b and S11, Supporting Information). We found that dimer nanoparticles were easily taken up by living cells and were still intact after incubating of 24 h. MTT results revealed that ND-AuNPs exhibited low cytotoxicity to HeLa cells. About 99% of HeLa cells were able to survive even up to a concentration of 1 pM, confirming their biocompatibility (Figures 5c). From the bright field images of the confocal fluorescence studies, we see that the appearance of a spreading cell has the shape of a "fried egg". This indicates that ND-AuNPs-treated HeLa cells were kept at good shape. These findings are highly significant for the use of dimers in biological applications.

Conclusion. In summary, we present a new ligand-induced self-assembly strategy for preparing ND-AuNP dimers via stable and strong noncovalent biotin−streptavidin linkage. In comparison to typical DNA-directed assembly strategies, this method is robust and scalable, allowing the synthesis of stable dual-functional nanoparticle hybrids that are capable of both heating and highly sensitive thermometry, thus offering an important step toward real-time controlled photothermal therapy with high therapeutic accuracy.[31] This programmed dimer fabrication of designed sizes and compositions is also potentially useful in materials science and engineering.

■ ASSOCIATED CONTENT

Supporting Information

The Supporting Information is available free of charge on the ACS Publications website at DOI: 10.1021/acs.nanolett.9b00113.

Experimental procedures and TEM characterization data (PDF)

■ AUTHOR INFORMATION

Corresponding Author

*E-mail: peggylo@cityu.edu.hk.

ORCID

Hongkun Park: 0000-0001-9576-8829

Pik Kwan Lo: 0000-0001-5255-1718

Notes

The authors declare no competing financial interest.

■ ACKNOWLEDGMENTS

This work was supported National Science Foundation of China (NSFC 21778043 and 21574109 to P.K.L.), Health and Medical Research Fund (HMRF 05160336 and 03141076 to P.K.L.), City University of Hong Kong (CityU 9680104, 7004655, and 7004911 to P.K.L.), US Army Research Office (W911NF-15-1-0548 to H.P. and M.L.), and the Gordon and Betty Moore Foundation (to H.P. and M.L.).

■ REFERENCES

(1) Xie, C.; Zhen, X.; Miao, Q.; Lyu, Y.; Pu, K. Self-Assembled Semiconducting Polymer Nanoparticles for Ultrasensitive Near-Infrared Afterglow Imaging of Metastatic Tumors. *Adv. Mater.* **2018**, *30* (21), 1801331.

(2) Xie, C.; Zhen, X.; Lyu, Y.; Pu, K. Nanoparticle Regrowth Enhances Photoacoustic Signals of Semiconducting Macromolecular Probe for In Vivo Imaging. *Adv. Mater.* **2017**, *29* (44), 1703693.

(3) Xie, C.; Zhen, X.; Lei, Q.; Ni, R.; Pu, K. Self-Assembly of Semiconducting Polymer Amphiphiles for In Vivo Photoacoustic Imaging. *Adv. Funct. Mater.* **2017**, *27* (8), 1605397.

(4) Jin, Y.; Jia, C.; Huang, S. W.; O'Donnell, M.; Gao, X. Multifunctional Nanoparticles as Coupled Contrast Agents. *Nat. Commun.* **2010**, *1* (4), 1−8.

(5) Wu, W.; Shen, J.; Banerjee, P.; Zhou, S. A Multifuntional Nanoplatform Based on Responsive Fluorescent Plasmonic ZnO-Au@PEG Hybrid Nanogels. *Adv. Funct. Mater.* **2011**, *21* (15), 2830−2839.

(6) Passeri, D.; Rinaldi, F.; Ingallina, C.; Carafa, M.; Rossi, M.; Terranova, M. L.; Marianecci, C. Biomedical Applications of Nanodiamonds: An Overview. *J. Nanosci. Nanotechnol.* **2015**, *15* (2), 972−988.

(7) Leung, H. M.; Chan, M. S.; Liu, L. S.; Wong, S. W.; Lo, T. W.; Lau, C.; Tin, C.; Lo, P. K. Dual-Function, Cationic, Peptide-Coated Nanodiamond Systems: Facilitating Nuclear-Targeting Delivery for Enhanced Gene Therapy Applications. *ACS Sustainable Chem. Eng.* **2018**, *6*, 9671−9681.

(8) Chan, M. S.; Liu, L. S.; Leung, H. M.; Lo, P. K. Cancer-Cell-Specific Mitochondria-Targeted Drug Delivery by Dual-Ligand-Functionalized Nanodiamonds Circumvent Drug Resistance. *ACS Appl. Mater. Interfaces* **2017**, *9* (13), 11780−11789.

(9) Slegerova, J.; Rehor, I.; Havlik, J.; Raabova, H.; Muchova, E.; Cigler, P. Nanodiamonds as Intracellular Probes for Imaging in Biology and Medicine. *Intracellular Delivery II* **2014**, *7*, 363.

DOI: 10.1021/acs.nanolett.9b00113
Nano Lett. 2019, 19, 2020−2026

(10) Maze, J. R.; Stanwix, P. L.; Hodges, J. S.; Hong, S.; Taylor, J. M.; Cappellaro, P.; Jiang, L.; Dutt, M. V. G.; Togan, E.; Zibrov, A. S.; et al. Nanoscale Magnetic Sensing with an Individual Electronic Spin in Diamond. *Nature* **2008**, *455* (7213), 644−647.
(11) Balasubramanian, G.; Chan, I. Y.; Kolesov, R.; Al-Hmoud, M.; Tisler, J.; Shin, C.; Kim, C.; Wojcik, A.; Hemmer, P. R.; Krueger, A.; et al. Nanoscale Imaging Magnetometry with Diamond Spins under Ambient Conditions. *Nature* **2008**, *455* (7213), 648−651.
(12) Wu, Y.; Jelezko, F.; Plenio, M. B.; Weil, T. Diamond Quantum Devices in Biology. *Angew. Chem., Int. Ed.* **2016**, *55* (23), 6586−6598.
(13) Sushkov, A. O.; Chisholm, N.; Lovchinsky, I.; Kubo, M.; Lo, P. K.; Bennett, S. D.; Hunger, D.; Akimov, A.; Walsworth, R. L.; Park, H.; et al. All-Optical Sensing of a Single-Molecule Electron Spin. *Nano Lett.* **2014**, *14* (11), 6443−6448.
(14) Sotoma, S.; Epperla, C. P.; Chang, H. C. Diamond Nanothermometry. *ChemNanoMat* **2018**, *4* (1), 15−27.
(15) Kucsko, G.; Maurer, P. C.; Yao, N. Y.; Kubo, M.; Noh, H. J.; Lo, P. K.; Park, H.; Lukin, M. D. Nanometre-Scale Thermometry in a Living Cell. *Nature* **2013**, *500* (7460), 54.
(16) Neumann, P.; Jakobi, I.; Dolde, F.; Burk, C.; Reuter, R.; Waldherr, G.; Honert, J.; Wolf, T.; Brunner, A.; Shim, J. H.; et al. High-Precision Nanoscale Temperature Sensing Using Single Defects in Diamond. *Nano Lett.* **2013**, *13* (6), 2738−2742.
(17) Schroeder, A.; Heller, D. A.; Winslow, M. M.; Dahlman, J. E.; Pratt, G. W.; Langer, R.; Jacks, T.; Anderson, D. G. Treating Metastatic Cancer with Nanotechnology. *Nat. Rev. Cancer* **2012**, *12* (1), 39−50.
(18) Xu, G.; Stevens, S. M.; Kobiessy, F.; Brown, H.; McClung, S.; Gold, M. S.; Borchelt, D. R. Identification of Proteins Sensitive to Thermal Stress in Human Neuroblastoma and Glioma Cell Lines. *PLoS One* **2012**, *7* (11), 1−13.
(19) Halas, N. J. Plasmonics: An Emerging Field Fostered by Nano Letters. *Nano Lett.* **2010**, *10* (10), 3816−3822.
(20) Abadeer, N. S.; Murphy, C. J. Recent Progress in Cancer Thermal Therapy Using Gold Nanoparticles. *J. Phys. Chem. C* **2016**, *120* (9), 4691−4716.
(21) Tsai, P. C.; Epperla, C. P.; Huang, J. S.; Chen, O. Y.; Wu, C. C.; Chang, H. C. Measuring Nanoscale Thermostability of Cell Membranes with Single Gold−Diamond Nanohybrids. *Angew. Chem., Int. Ed.* **2017**, *56* (11), 3025−3030.
(22) Liu, Y. L.; Sun, K. W. Plasmon-Enhanced Photoluminescence from Bioconjugated Gold Nanoparticle and Nanodiamond Assembly. *Appl. Phys. Lett.* **2011**, *98* (15), 153702.
(23) Liu, W.; Naydenov, B.; Chakrabortty, S.; Wuensch, B.; Hübner, K.; Ritz, S.; Cölfen, H.; Barth, H.; Koynov, K.; Qi, H.; et al. Fluorescent Nanodiamond-Gold Hybrid Particles for Multimodal Optical and Electron Microscopy Cellular Imaging. *Nano Lett.* **2016**, *16*, 6236−6244.
(24) Zhang, B.; Fang, C.-Y.; Chang, C.-C.; Peterson, R.; Maswadi, S.; Glickman, R. D.; Chang, H.-C.; Ye, J. Y. Photoacoustic Emission from Fluorescent Nanodiamonds Enhanced with Gold Nanoparticles. *Biomed. Opt. Express* **2012**, *3* (7), 1662−1629.
(25) Hurst, S. J.; Lytton-Jean, A. K. R.; Mirkin, C. A. Maximizing DNA Loading on a Range of Gold Nanoparticle Sizes. *Anal. Chem.* **2006**, *78* (24), 8313−8318.
(26) Lim, D. K.; Jeon, K. S.; Kim, H. M.; Nam, J. M.; Suh, Y. D. Nanogap-Engineerable Raman-Active Nanodumbbells for Single-Molecule Detection. *Nat. Mater.* **2010**, *9* (1), 60−67.
(27) Maye, M. M.; Nykypanchuk, D.; Cuisinier, M.; Van Der Lelie, D.; Gang, O. Stepwise Surface Encoding for High-Throughput Assembly of Nanoclusters. *Nat. Mater.* **2009**, *8* (5), 388−391.
(28) Kucsko, G.; Maurer, P. C.; Yao, N. Y.; Kubo, M.; Noh, H. J.; Lo, P. K.; Park, H.; Lukin, M. D. Nanometre-Scale Thermometry in a Living Cell. *Nature* **2013**, *500* (7460), 54−58.
(29) Cebik, J.; McDonough, J. K.; Peerally, F.; Medrano, R.; Neitzel, I.; Gogotsi, Y.; Osswald, S. Raman Spectroscopy Study of the Nanodiamond-to-Carbon Onion Transformation. *Nanotechnology* **2013**, *24* (20), 205703.
(30) Amendola, V.; Pilot, R.; Frasconi, M.; Maragò, O. M.; Iatì, M. A. Surface Plasmon Resonance in Gold Nanoparticles: A Review. *J. Phys.: Condens. Matter* **2017**, *29* (20), 203002.
(31) Suo, H.; Zhao, X.; Zhang, Z.; Guo, C. 808 Nm Light-Triggered Thermometer−Heater Upconverting Platform Based on Nd 3+ -Sensitized Yolk−Shell GdOF@SiO 2. *ACS Appl. Mater. Interfaces* **2017**, *9* (50), 43438−43448.

DOI: 10.1021/acs.nanolett.9b00113
Nano Lett. 2019, 19, 2020−2026